

# CAVITY-BASED FREE-ELECTRON LASER RESEARCH AND DEVELOPMENT: A JOINT ARGONNE NATIONAL LABORATORY AND SLAC NATIONAL LABORATORY COLLABORATION

G. Marcus, F.-J. Decker, G. L. Gassner, A. Halavanau, J. Hastings, Z. Huang, Y. Liu, J. MacArthur, R. Margraf, T. Raubenheimer, A. Sakdinawat, T. Tan, D. Zhu, SLAC National Accelerator Laboratory, Menlo Park, CA 94025, USA

J. W. J. Anton, L. Assoufid, K. Goetze, W. Jansma, S. Kearney, K.-J. Kim, R. Lindberg, A. Miceli, X. Shi, D. Shu, Y. Shvyd'ko, J. P. Sullivan, M. White, Argonne National Laboratory, Argonne, IL 60439, USA  
B. Lantz, Stanford University, Stanford, CA 94305, USA

## Abstract

One solution for producing longitudinally coherent FEL pulses is to store and recirculate the output of an amplifier in an X-ray cavity so that the X-ray pulse can interact with following fresh electron bunches over many passes. The X-ray FEL oscillator (XFEL) and the X-ray regenerative amplifier FEL (XRA FEL) concepts use this technique and rely on the same fundamental ingredients to realize their full capability. Both schemes require a high repetition rate electron beam, an undulator to provide FEL gain, and an X-ray cavity to recirculate and monochromatize the radiation. The shared infrastructure, complementary performance characteristics, and potentially transformative FEL properties of the XFEL and XRA FEL have brought together a joint Argonne National Laboratory (ANL) and SLAC National Laboratory (SLAC) collaboration aimed at enabling these schemes at LCLS-II. We present plans to install a rectangular X-ray cavity in the LCLS-II undulator hall and perform experiments employing 2-bunch copper RF linac accelerated electron beams. This includes performing cavity ring-down measurements and 2-pass gain measurements for both the low-gain XFEL and the high-gain XRA FEL schemes.

## INTRODUCTION

The incontrovertible success of the world's first hard X-ray free-electron laser (XFEL), LCLS [1], has led to a significant increase in the global FEL capacity. Additional facilities in Japan, Germany, Switzerland, Korea and China are either planned or are currently operating. These light sources, based primarily on Self-Amplified Spontaneous Emission (SASE) [2], are capable of producing extremely bright, transversely coherent, ultra-short X-ray pulses that have opened the door to new regimes of photon science [3, 4]. They have revolutionized the study of chemistry, physics, biology, and many other related fields of science and technology. Single-pass SASE FEL amplifiers, however, suffer from poor longitudinal coherence due to the stochastic nature of the start-up process. The improvement of the FEL longitudinal coherence and the ability to trade off peak power, average power, pulse duration, and bandwidth is of great practical importance [5].

Longitudinal coherence can be obtained by seeding an FEL amplifier with narrow bandwidth radiation well above

the effective shot noise power in the electron beam. Examples of this include self-seeding [6, 7], which has been successfully implemented at LCLS in both the hard [8] and soft [9] X-ray spectral regions. Variations on this concept are also being studied [10, 11]. Self-seeding, however, nominally suffers from low seed power in an attempt to preserve the electron beam properties important for lasing and is fundamentally still dependent on the noisy SASE process leading to large (potentially 100%) seed power fluctuations.

Another leading candidate for obtaining longitudinal coherence leverages an X-ray cavity to monochromatize and store a fraction of a recirculating X-ray pulse so that it can interact with following fresh electron bunches over many passes. These so-called cavity-based X-ray free-electron lasers (CBXFELs) include the X-ray free-electron laser oscillator (XFEL) [12] and the X-ray regenerative amplifier free-electron laser (XRA FEL) [13]. In the past, these concepts were not feasible at X-ray FEL facilities because of the lack of high-reflectivity X-ray cavity mirrors and because of the limited repetition rate of the normal conducting technologies responsible for the production and acceleration of the electron bunches delivered to the undulator. The progress in achieving high-reflectivity diamond crystal mirrors in the hard x-ray regime [14–16] and in superconducting technology adopted by LCLS-II [17, 18] and LCLS-II-HE [19], however, will be capable of supporting steady-state repetition rates up to  $\sim 1$  MHz, making the footprint of the recirculating optical cavity reasonable.

The XFEL and XRA FEL concepts rely on the same fundamental ingredients to realize their full capability. Each scheme requires a high repetition rate electron beam, an undulator to provide FEL gain, and an X-ray optical cavity to recirculate and monochromatize the X-ray radiation. While the XFEL and XRA FEL schemes share a common infrastructure, they target different but complementary FEL performance characteristics. The XFEL relies on a low-loss cavity supporting a low-gain FEL for ultra-narrow bandwidth while the XRA FEL leverages a high-gain FEL interaction that can support much larger radiation output coupling.

As an example of the difference between the two CBXFEL schemes, Table 1 shows a semi-qualitative comparison of operational characteristics while Table 2 shows the typical hard X-ray (HXR) performance characteristics that are ex-

pected for SASE, XRAFEL, and XFEL at LCLS-II/HE.

Table 1: Semi-Qualitative Comparison Between the XRAFEL and XFEL Schemes

	XRAFEL	XFEL
Gain & output coupling	High	Low
Necessary cavity roundtrip efficiency	~ 1 %	~ 85%
Passes to saturation	~ 10's	~ 100's
Repetition rate	Q-switched (~10-50 kHz), CW (~ MHz)	CW (~ MHz)

The XFEL can produce temporally long and coherent pulses with extremely stable and ultra-narrow bandwidths that ultimately result in X-rays that are roughly three orders of magnitude higher in average brightness than that of SASE at LCLS-II/HE. The XRAFEL system, conversely, aims at the production of longitudinally coherent but shorter FEL pulses that can result in both high average and peak brightness (Q-switched) X-rays.

The shared infrastructure, complementary performance characteristics, and transformative FEL properties of the two CBXFEL schemes has brought together a joint ANL/SLAC collaboration aimed at enabling these schemes at LCLS-II and the LCLS-II-HE upgrade. The primary objective of this collaboration is the construction of a rectangular X-ray cavity around the first seven LCLS-II HXR undulator sections (see Figure 1a), allowing for the investigation of crucial aspects related to CBXFEL physics using a pair of electron bunches (sub  $\mu$ s separation) from the SLAC copper (Cu) RF linac. The experimental program includes two-pass gain measurements as well as cavity ring-down measurements for both the low-gain XFEL and the high-gain XRAFEL schemes. We envision this as a three-year project with the possibility for schedule contingency of an extra year driven largely by the LCLS-II commissioning and downtime schedules. Future studies using electron bunches from the high repetition rate accelerator will be possible after appropriate cavity upgrades are made.

## EXPERIMENTAL SETUP

Figure 1a shows a mockup (top view) of a potential rectangular X-ray cavity in the LCLS-II undulator hall while Figure 1b shows a cartoon version with the electron and photon paths noted. Four motion stacks will form the basis of the optical cavity that in turn will mount four HPHT-IIa diamond crystal plates in strain free holders. The first two crystal plates reflect the X-ray pulse into and out of the undulator line using the (400) Bragg reflection and will be located in the middle of the four-dipole electron beam delay chicanes that bracket the seven undulator sections. Two additional crystals reflect the X-ray pulse back to the electron path in the undulator. To control the transverse

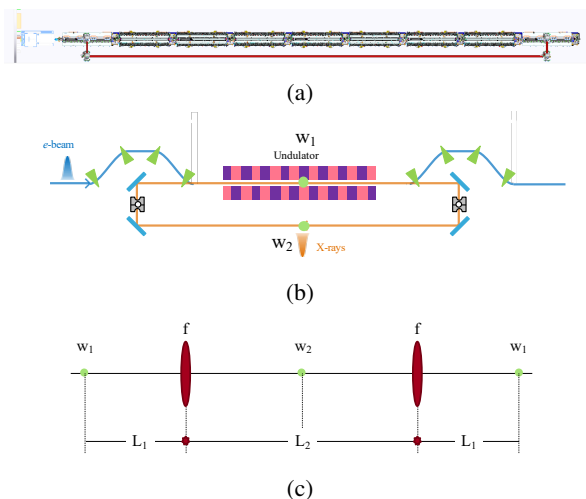


Figure 1: (a) Top view of the rectangular cavity as envisioned. From left to right in the undulator beamline: TDUND, chicane and optics chamber, 7 HXR undulators, chicane and optics chamber. The solid red line illustrates the X-ray cavity return line. Not shown are two CRLs on the short ends of the rectangle (see (b) below). (b) Cartoon of the CBXFEL concept showing the paths of the electrons and photons. (c) Equivalent unfolded optical lattice of the X-ray cavity in (b) above.

cavity mode, two paraboloidal compound refractive lenses (CRLs) made of Beryllium [20–22] will be placed symmetrically in the short arms of the rectangle. The motion stacks will include nanoradian-level-resolution positioning stages. The diamonds deployed in this cavity will be cut parallel to the (100) crystal surface, where the bulk of previous R&D has been performed, and high-quality diamond samples can be fabricated by multiple vendors (see [23] for a recent review). A long-range laser interferometer system, along with additional X-ray diagnostics, will be used for alignment, characterization, and stabilization of the cavity. A non-destructive in-situ diagnostic line will include high-resolution measurements of the X-ray transverse profile. The XFEL/XRAFEL cavity design will include sufficient diagnostics to enable the required precision angular alignment to be accomplished [24].

## TOLERANCES OF THE X-RAY CAVITY

Figure 1c shows the equivalent unfolded optical lattice of the X-ray cavity in Figure 1b including focusing elements provided by compound refractive lenses (CRLs). This symmetric system has a waist at two locations,  $w_1$  and  $w_2$  as noted in the figure. The coupling between the electron beam and the X-rays is typically optimized in the low-gain XFEL scenario when the radiation waist is in the middle of the undulator, as it is here, and when  $Z_R \approx \langle \beta \rangle$ , where  $Z_R$  is the X-ray pulse Rayleigh length and  $\langle \beta \rangle$  is the average beta function of the electron beam in the undulator. Table 3 shows the undulator and cavity parameters for the proposed experimental setup. An electron beam energy of  $\sim 10.3$  GeV

Table 2: Projected HXR Performance Characteristics at the High Repetition Rate LCLS-II/HE from SASE, XRFEL, and XFEL

	SASE	XRFEL	XFEL
Peak Power	~10 GW	~50 GW	~100 MW
Average power	~100 W (at 1 MHz)	10 W (at 10 kHz)	20 W (at 1 MHz)
Spectral bandwidth	~10 eV	~0.1 eV	~1 meV
Pulse length	~ 1 – 100 fs	~ 20 fs	~ 1 ps
Stability	Poor	Excellent	Excellent
Longitudinal coherence	Poor	Excellent	Excellent
Transverse mode	Defined by gain-guiding	Defined by gain-guiding	Defined by the optical cavity

Table 3: Major Undulator and Cavity Parameters

Parameter	Value	Unit
<b>Undulator</b>		
Period	2.6	cm
Number of segments	7	-
Periods per segment	130	-
Length	28	m
K	2.44	-
<b>Cavity</b>		
Crystal material	C*(400)	-
Bragg angle	45	degree
Photon energy	9.83	keV
Wavelength	1.26	Angstrom
Bragg width (energy)	75	meV
Bragg width (angle)	8	μrad
Total length	~66	m

is needed to support the gain of 9.83 keV photons in the LCLS-II HXR undulator. This, in turn, yields an  $\langle \beta \rangle \approx 22$  m for a matched electron bunch in the strong focusing undulator FODO lattice and a matched waist size  $w_1 \approx 30 \mu\text{m}$ . Commercially available beryllium CRLs with a focal length of 28.4 m (at a 9.83 keV photon energy) produce a waist size of  $w_1 \approx 32 \mu\text{m}$ , which is close to the matched solution.

As an initial approximation, if the error in mirror angles are independent and random, a statistical tolerancing analysis using the Root Sum Square (RSS) method can be performed to estimate the required stability of the motion stacks. In this method, the total error in displacement at the undulator entrance after propagation through the optical cavity can be

written as

$$\Delta_{tot} = c_1\theta_{m1} + c_2\theta_{m2} + c_3\theta_{m3} + c_4\theta_{m4}, \quad (1)$$

where the  $c_i$  are functions of the optical cavity parameters (drift lengths, focal lengths, etc.) and the  $\theta_{mi}$  are the individual mirror angular errors. The total RMS error in the displacement, assuming independent and equal magnitude mirror errors ( $\sigma_{mi} = \sigma_m$ ), can then be found by propagation in the usual sense as

$$\sigma_{tot} = \sqrt{(c_1^2 + c_2^2 + c_3^2 + c_4^2)\sigma_m^2}. \quad (2)$$

Setting the tolerance as  $\pm TOL = \pm 3\sigma_{tot}$ , one can then find the mirror RMS fluctuations that results in an unlikely  $3\sigma_{tot}$  ( $\sim 0.27\%$  chance) event to occur. If the tolerance is set such that the trajectory deviation is one half the RMS electron beam size at the entrance to the undulator ( $TOL = \sigma_e/2$ ), the RMS fluctuation in the mirror angles must be less than  $\sim 55$  nrad. This is routinely realized in precision x-ray optics mechanisms. These tolerances should be relaxed for the XRFEL due to gain-guiding of the radiation during high-gain amplification.

The use of this statistical tolerancing method is somewhat questionable given the small number of independent sources of error (there are only four mirrors). Therefore, both the high and low gain two-pass systems are being evaluated with time-dependent and three-dimensional FEL simulations using genesis [25] and Fourier optics propagation of the resulting fields through the optical cavity.

## TWO-BUNCH CURF ELECTRON BEAM DYNAMICS

The high-brightness electron beams from the CuRF linac have been successfully supporting the high-gain SASE FEL for the past 10 years at LCLS and are well characterized [26]. Beam shaping is employed to ensure a uniform longitudinal phase space (LPS) at the entrance to the undulator [27]. An example of two typical electron beam LPS's is shown in

Content from this work may be used under the terms of the CC BY 3.0 licence (© 2019). Any distribution of this work must maintain attribution to the author(s), title of the work, publisher, and DOI

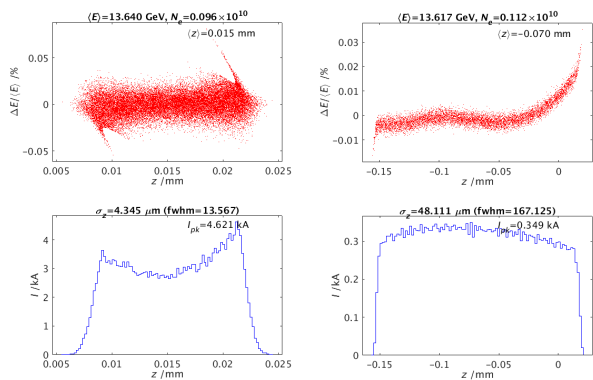


Figure 2: Typical longitudinal phase space (top) and current profile (bottom) of a high peak current (left) and low peak current (right) high-brightness electron beam at the entrance to the HXR undulator from the CuRF linac (LiTrack simulations).

Figure 2. Here, LiTrack [28] simulations show that a  $\sim 150$  pC charge electron beam that is  $\sim 50$  fs long can have a peak current of  $\sim 3$  kA, an RMS energy spread of 1.5 MeV, and a slice emittance of  $\sim 0.6$  mm-mrad (left). Electron beams similar to this are deployed in regular operation. Low peak current solutions are also possible. LiTrack simulations show that a 180 pC charge electron beam that is  $\sim 300$  fs long in the core can have a peak current of  $\sim 300$  A, a slice RMS energy spread in the core of  $\sim 150$  keV, and a slice-emittance of  $\sim 0.5$  mm-mrad (right). These solutions should be more than sufficient to demonstrate both low and high two-pass gain.

Two-bunch operation using the CuRF linac has been demonstrated in the past [29] for various relative delays between the two electron bunches ranging from a few ns to  $\sim 210$  ns. Two bunches are generated by two independent lasers impinging on the photoinjector cathode. Their relative charge difference can be controlled to about the 1% level, their individual time separation can be adjusted with a precision of 0.07 ps, and their RMS temporal separation jitter can be controlled to less than 17 fs [30,31]. In order to control and remove the energy difference between the two bunches, one can introduce a small phase difference in the second section of the CuRF linac.

The optical cavity in the undulator hall will have a round trip length of  $\sim 66$  m requiring a relative delay between the electron beams of  $\sim 220$  ns. Two-bunch spacing of 210 ns (600 RF wavelengths) for the high peak current scenario has been achieved in the past. The FEL performance in this case nearly achieved twice the single bunch performance.

Ideally, the electron bunches need to be spatially and angularly aligned in the undulator to within a fraction of the electron bunch transverse size over the length of the undulator. Addressing this alignment requires additional R&D and infrastructure. In the past, the demonstrated two-bunch mode of operation typically provided two different electron beam energies at the entrance of the undulator to produce FEL photons at two different photon energies. This

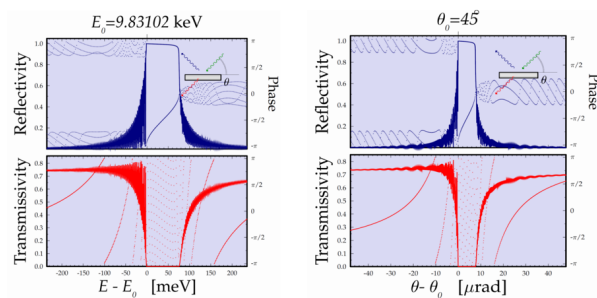


Figure 3: Bragg reflectivity of diamond crystals in the (400) reflection as a function of the photon energy and angular deviation ( $E_0 = 9.83$  keV,  $\theta_0 = 45^\circ$ ).

enabled the use of dispersion bumps to control the relative alignment of the electron bunch trajectories to within 5-10% of the transverse size. This technique will not be possible for two bunches of equal energy. In addition, transverse long range wakefields, introduced by the first bunch and acting on the second bunch, have to be compensated to ensure closed orbits in the undulators. Therefore, four ultra-fast strip-line kickers will be installed in the LTU to independently control the four transverse coordinates ( $x, x', y, y'$ ) of each electron bunch.

## TWO-PASS GAIN MEASUREMENTS

As previously mentioned, a rectangular X-ray cavity will be constructed around the first seven sections of the LCLS-II HXR undulator, formed by four diamond crystals (see Figure 1 above). A rectangular cavity configuration, rather than a tunable zig-zag geometry [32], is adopted here based on the limited transverse space available in the undulator hall. The photon energy and corresponding wavelength, determined from the required  $45^\circ$  Bragg angle and the symmetric (400) diamond crystal reflection plane, are 9.83 keV and 1.26  $\text{\AA}$ , respectively. The Bragg reflection curves as a function of photon energy and angular deviation from  $45^\circ$  are shown in Figure 3. The two-pass gain measurements that will be made as part of this experimental program and that utilize the infrastructure mentioned above will proceed as follows. The normal conducting SLAC photoinjector and accelerator will produce two electron bunches that are spaced by  $\sim 220$  ns, which is set by the cavity round-trip time. The first electron bunch produces radiation that is monochromatized and returned to the entrance of the undulator so that it can interact with the following electron bunch. This experiment will test the key enabling aspects of any CBXFEL - the operation of an X-ray cavity that can store an X-ray pulse produced by an electron bunch and that the pulse can be amplified by another electron bunch. Performance estimates for both the low-gain and high-gain systems are discussed below. These estimates are based on the undulator and cavity parameters listed in Table 3 and the electron bunch parameters mentioned above.

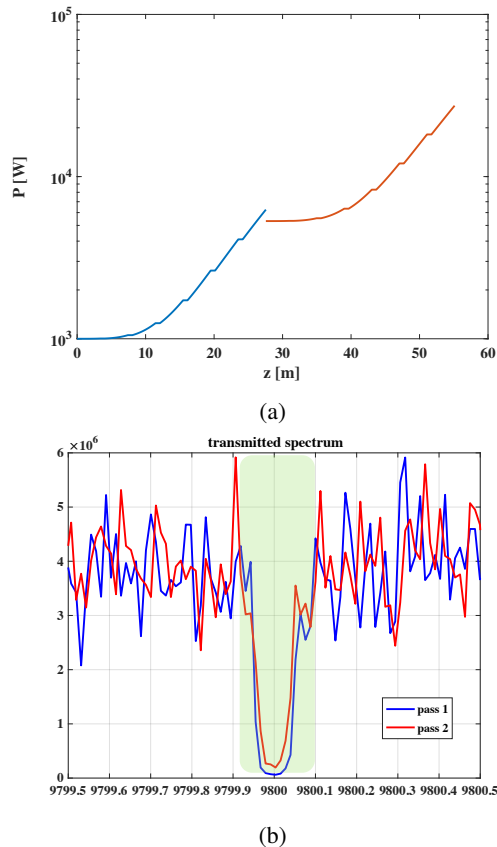


Figure 4: (a) Single-frequency (time-independent) simulations showing the two-pass gain for the low-gain XFEL scenario. (b) View of the average transmitted spectrum over 25 time-dependent simulations near the resonant photon energy. The spectral region of interest is highlighted in green.

### Low-Gain (XFEL) Measurements

Previous estimates have predicted that the number of photons produced by the first bunch, monochromatized, and deflected into the cavity, is  $N_\gamma = 5.8 \times 10^4$  and that the maximum intensity gain should be at least a factor of two [24]. Additional studies have since been performed using detailed genesis simulations. Figure 4a shows the results of relatively simple time-independent simulations showing two-pass gain. In this case, the results of the single-frequency simulation are simply fed back into the simulation of the second pass while the expected cavity roundtrip efficiency is used to scale the pulse power. The propagation of the radiation wavefront through the cavity has been ignored. The second pass gain is found to be  $\sim 5$  at the optimal detuning.

Figure 4b shows the transmitted spectrum of passes 1 and 2 averaged over 25 shots for time-dependent simulations. In this case, the reflection curves of Figure 3 are used to filter the first pass radiation both in photon energy and angle. The output coupling diamond crystal in this case is assumed to be  $20 \mu\text{m}$  thick and manufactured using a drumhead technique [33]. The full three-dimensional radiation field is propagated through the cavity using Fourier optics techniques. The gain

of the second pass relative to the first pass in the spectral region of interest is  $\sim 3.15$  and agrees remarkably well with the single-frequency results. There were no cavity errors in this case. Future work will include cavity mirror angular errors and will be used to compare against the analytical results presented above and to define the tolerances on the angular stability of the cavity optical system.

### High-Gain (XRFEL) System

A similar numerical analysis of the high-gain system was also performed. For brevity, the figures are not shown here. Time-independent simulations predict that the second pass gain through the system will be  $\sim 85$  while time-dependent simulations including propagation of the three-dimensional fields through the cavity show the gain of the second pass over the first in the spectral region of interest to be  $\sim 100$ .

## DISCUSSION

The successful implementation of a CBXFEL configuration is predicated on a high repetition rate electron beam and a high precision X-ray cavity. LCLS-II and the LCLS-II-HE upgrade will be capable of delivering electron bunch repetition rates as high as  $\sim 1$  MHz to the HXR undulator. It has been established that diamond crystals have the requisite properties to handle the high average and peak thermal load of the stored cavity X-ray power for both the XFEL and XRFEL concepts. Beam dynamics modeling and options for X-ray cavity output coupling for an XFEL and XRFEL are under active investigation and development. However, an FEL-scale optical cavity in the HXR spectral range has yet to be demonstrated. The project presented here addresses the joint ANL/SLAC collaboration strategy by conducting targeted R&D on the X-ray cavity infrastructure, exploring the physics of the XFEL and XRFEL schemes with real experiments, and demonstrating the necessary performance tolerances needed to realize a full-scale CBXFEL implementation.

## ACKNOWLEDGEMENTS

This work was supported by U.S. Department of Energy Contract No. DE-AC02-76SF00515.

## REFERENCES

- [1] P. Emma, *et al.*, “First lasing and operation of an angstrom-wavelength free-electron laser,” *Nat. Phot.*, vol. 4, pp. 641, 2010. doi:10.1038/nphoton.2010.176
- [2] R. Bonifacio, C. Pellegrini, and L. M. Narducci, “Collective instabilities and high-gain regime in a free electron laser,” *Opt. Comm.*, vol. 50, pp. 373, 1984. doi:10.1016/0030-4018(84)90105-6
- [3] C. Bostedt, *et al.*, “Ultra-fast and ultra-intense x-ray sciences: first results from the Linac Coherent Light Source free-electron laser,” *J. of Phys. B: Atomic, Molecular and Optical Physics*, vol. 46, pp. 164003, 2013. doi:10.1088/0953-4075/46/16/164003

- [4] Christoph Bostedt, *et al.*, “Linac Coherent Light Source: the first five years,” *Rev. of Mod. Phys.*, vol. 88, pp. 015007, 2016. doi:10.1103/RevModPhys.88.015007
- [5] R. W. Schoenlein, *et al.*, “New science opportunities enabled by LCLS-II x-ray lasers,” SLAC, Menlo Park, CA, SLAC-R-1053, 2015.
- [6] J. Feldhaus, *et al.*, “Possible application of X-ray optical elements for reducing the spectral bandwidth of an X-ray SASE FEL,” *Opt. Comm.*, vol. 140, pp. 341, 1997. doi:10.1016/S0030-4018(97)00163-6
- [7] G. Geloni, V. Kocharyanb and E. Saldin, “A novel self-seeding scheme for hard x-ray FELs,” *J. of Mod. Opt.*, vol. 58, pp. 1391, 2011. doi:10.1080/09500340.2011.586473
- [8] J. Amann *et al.*, “Demonstration of self-seeding in a hard-X-ray free-electron laser,” *Nat. Phot.*, vol. 6, pp. 693, 2012. doi:10.1038/nphoton.2012.180
- [9] D. Ratner *et al.*, “Experimental demonstration of a soft x-ray self-seeded free-electron laser,” *Phys. Rev. Lett.*, vol. 114, pp. 054801, 2015. doi:10.1103/PhysRevLett.114.054801
- [10] A. Halavanau, *et al.*, “High Power and Brightness Double Bunch LCLS-II,” presented at 39<sup>th</sup> Int. Free-Electron Laser Conf., Hamburg, 2019, THP071.
- [11] I. Inoue, *et al.*, “Generation of narrow-band x-ray free-electron laser via reflection self-seeding,” *Nat. Phot.*, 13, pp. 319, 2019. doi:10.1038/s41566-019-0365-y
- [12] K.-J. Kim, Y. Shvyd’ko, and Sven Reiche, “A proposal for an x-ray free-electron laser oscillator with an energy-recovery linac,” *Phys. Rev. Lett.* vol. 100, pp. 244802, 2008. doi:10.1103/PhysRevLett.100.244802
- [13] Z. Huang and R.D. Ruth, “Fully coherent x-ray pulses from a regenerative-amplifier free-electron laser,” *Phys. Rev. Lett.* vol. 96, pp. 144801, 2006. doi:10.1103/PhysRevLett.96.144801
- [14] Yu. Shvyd’ko, *et al.*, “High-reflectivity high-resolution x-ray crystal optics with diamonds,” *Nat. Phys.*, 6, pp. 196, 2010. doi:10.1038/nphys1506
- [15] Yuri Shvyd’ko, *et al.*, “Near-100% Bragg reflectivity of x-rays,” *Nat. Phot.* 5, pp. 539, 2011. doi:10.1038/nphoton.2011.197
- [16] T. Kolodziej, *et al.*, “High Bragg reflectivity of diamond crystals exposed to multi-kW mm<sup>2</sup> x-ray beams,” *J. of Synch. Rad.*, vol. 25, pp. 1022, 2018. doi:10.1107/S1600577518007695
- [17] T.O. Raubenheimer, ed., “LCLS-II final design report,” SLAC, Menlo Park, CA, LCLSII-1.1-DR-0251-R0, 2015.
- [18] T.O. Raubenheimer, “Technical challenges of the LCLS-II CW x-ray FEL,” in *Proc. 6<sup>th</sup> Int. Particle Accelerator Conf.*, Virginia, USA, 2015. doi:10.18429/JACoW-IPAC2015-WEYC1
- [19] T.O. Raubenheimer, “The LCLS-II-HE, a high energy upgrade of the LCLS-II,” 60<sup>th</sup> *ICFA Advanced Beam Dynamics Workshop on Future Light Sources*, Shanghai, China, 2018. doi:10.18429/JACoW-FLS2018-MOP1WA02
- [20] A. Snigirev, *et al.*, “A compound refractive lens for focusing high-energy x-rays,” *Nature*, 384, pp. 49-51, 1996. doi:10.1038/384049a0
- [21] B. Lengeler, *et al.*, “Imaging by parabolic refractive lenses in the hard x-ray range,” *J. Synchrotron Rad.*, 6, pp. 1153, 1999. doi:10.1107/S0909049599009747
- [22] T. Kolodziej, *et al.*, “Efficiency and coherence preservation studies of Be refractive lenses for XFEL application,” *J. Synchrotron Rad.*, 25, pp. 354 2018. doi:10.1107/S160057751701699X
- [23] Yu. Shvyd’ko, *et al.*, “Diamond x-ray optics: transparent, resilient, high-resolution, and wavefront preserving,” *MRS Bulletin*, 42, pp. 437, 2017. doi:10.1557/mrs.2017.119
- [24] K.-J. Kim, *et al.*, “Test of an x-ray cavity using double-bunches from the LCLS Cu-linac,” *Proc. of the 10<sup>th</sup> Int. Particle Accelerator Conf.*, Melbourne, 2019, TUPRB096. doi:10.18429/JACoW-IPAC2019-TUPRB096
- [25] S. Reiche, “GENESIS 1.3: a fully 3D time-dependent FEL simulation code,” *Nucl. Instr. Meth. Phys. Res. Sec. A*, vol. 429, pp. 243, 1999. doi:10.1016/S0168-9002(99)00114-X
- [26] C. Behrens, *et al.*, “Few-femtosecond time-resolved measurements of X-ray free-electron lasers,” *Nat. Comm.*, vol. 5, pp. 3762, 2014. doi:10.1038/ncomms4762
- [27] Y. Ding, *et al.*, “Beam shaping to improve the free-electron laser performance at the Linac Coherent Light Source,” *Phys. Rev. Accel. and Beams*, vol. 19, pp. 100703, 2016. doi:10.1103/PhysRevAccelBeams.19.100703
- [28] K. Bane and P. Emma, “LiTrack: a fast longitudinal phase space tracking code with graphical user interface,” in *Proc. of the 21<sup>st</sup> Particle Accelerator Conf.*, Knoxville, TN, 2005, FPAT091.
- [29] F.-J. Decker, *et al.*, “A Demonstration of Multi-Bunch Operation in the LCLS,” in *Proc. of the 32<sup>nd</sup> Int. Free-Electron Laser Conf.*, Malmö, Sweden, 2010, WEPB33.
- [30] F.-J. Decker, *et al.*, “Recent developments and plans for two bunch operation with up to 1  $\mu$ s separation at LCLS,” SLAC, Menlo Park, CA, SLAC-PUB-17128, 2018.
- [31] F.-J. Decker, private communication, 2019.
- [32] K.-J. Kim and Y. Shvyd’ko, “Tunable optical cavity for an x-ray free-electron-laser oscillator,” *Phys. Rev. ST Accel. Beams.*, vol. 12, pp. 030703, 2009. doi:10.1103/PhysRevSTAB.12.030703
- [33] Tomasz Kolodziej, *et al.*, “Diamond drumhead crystals for x-ray optics applications,” *J. of Appl. Cryst.*, vol. 49, pp. 1240, 2016. doi:10.1107/S1600576716009171